

The Role of Climatological State on Driving US Heat Waves Through Rossby Waves Packets

Valentina Castañeda¹, Lei Wang¹

¹Department of Earth, Atmospheric, and Planetary Sciences, Purdue University

Key Points:

- The climatological state drives the stationary Rossby wave propagation providing critical dynamical conditions for heat waves in the US.
- A dry atmospheric model with a corrected climatological state generates heatwaves that are statistically consistent with observations.
- The slowly propagating Rossby wave packets with a timescale of 20-30 days can be a source of intraseasonal predictability.

Corresponding author: Lei Wang, leiwang@purdue.edu

Abstract

While heat waves are local extreme weather events, a planetary Rossby wave pattern is statistically related to the occurrence of heat waves events in the U.S. However, whether such planetary wave patterns cause the enhanced statistics of local heat waves or as a coincidence is debatable. In this work, we hypothesize that the atmospheric climatological state dictates the slowly propagating wave pattern, which sets up a conducive large-scale environment for local US heat waves. We implement an idealized dry dynamic core model with an iterative approach to simulate the realistic North American summer climatological state. As the model can generate similar large-scale planetary wave patterns propagating throughout North America, significantly more heatwaves are generated, and the statistics of heat waves become consistent with that estimated in reanalysis products. The slowly propagating Rossby wave packets with a timescale of 20-30 days can serve as a new source of intraseasonal predictability.

Plain Language Summary

Heatwaves are the leading weather-related killer in the United States and affect mainly the most vulnerable communities. These extreme events are statistically related to a large-scale wave pattern of Rossby waves that features a zonal wavenumber five structure. To find out what controls this wave pattern, we use a simple general circulation model that only contains dry dynamics without complicated interactions with moisture or clouds. We found that by modifying the climatological state of temperature and velocity fields based on the observed structure from the Northern Hemisphere summer, we can observe the same wave number five pattern developing days before the heatwave events, resembling that from the observations. This result suggests that the climatological state of the Northern Hemispheric summer provides a conducive environment for heatwaves in the U.S. due to the slowed-down propagation speed of the Rossby wave packets. A deeper understanding of its dynamics is crucial because, as this pattern develops up to 20 days ahead of the extremes, the underlying physical process governing this pattern may serve as a source of predictability on the Subseasonal-to-Seasonal (S2S) timescale, a current gap of forecasts between weather and climate.

1 Introduction

Over the coming century, climate change is expected to increase average summer temperatures and the severity of extreme heat linked with heat waves events. In the United States, the frequency, intensity, and duration of heat waves have been increasing rapidly in recent decades, and this behavior is projected to continue in the next decades (Meehl & Tebaldi, 2004). Currently, forecasters in the United States can only predict extreme events up to 10 days in advance because, unlike in the tropics, circulation in the mid-latitudes is more chaotic as it is dominated by climatic noise (Feldstein, 2000).

However, it is intriguing to hypothesize that certain atmospheric circulation states can be substantially more predictable than the average scenario, because these circulation regimes are associated with low-frequency patterns (Schubert et al., 2011). With this in mind, and considering that different studies have suggested that propagating stationary Rossby Waves play an important role in the mid-latitude atmospheric variability, the scientific community recently has increased interest in the connection between extreme weather events and large-scale atmospheric patterns such as Rossby Wave Packets (Chen & Newman, 1998; Schubert et al., 2011; Fragkoulidis & Wirth, 2020).

In many of the investigated cases, the extreme weather was linked to an upper-tropospheric trough (i.e., a breaking Rossby Waves). For example, Chen and Newman (1998) suggests that Rossby Waves originating in the west Pacific were the key in initiating intense anomalous anticyclones during the 1988 U.S. drought. Also, Schubert et al. (2011) relates this

61 large-scale pattern with monthly mean precipitation and surface temperature variabil-
 62 ity over many regions of the extratropical land areas, including the northern U.S., parts
 63 of Canada, Europe, and Russia. Following the same approach, Ding and Wang (2005)
 64 found an interannually varying Northern Hemisphere circumglobal pattern with a pre-
 65 ferred wavenumber five structure. This particular structure is confined within the wave-
 66 guide associated with the summer north jet stream in the stationary state and is linked
 67 to significant surface air temperature and rainfall anomalies in western Europe, Euro-
 68 pean Russia, India, East Asia, and North America. In a more recent study Teng et al.
 69 (2013), more concrete evidence has been shown of the relationship between the occur-
 70 rence of heatwaves in the U.S. and the same wavenumber five pattern developing as early
 71 as 20 days ahead of the events. Despite the growing evidence for the concurrences of this
 72 interesting wave number five pattern, the physical mechanism that drives the atmospheric
 73 pattern and thus determines heatwaves has yet to be understood.

74 This study aims to understand better the fundamental role of atmospheric dynam-
 75 ics in the evolution of U.S. heat waves based on the hypothesis that the climatological
 76 state for the Northern Hemisphere summer drives the stationary Rossby wave propaga-
 77 tion providing critical dynamical conditions for heat waves in the U.S. Inspired by the
 78 motivation to look for the simplest possible model in the climate model hierarchies (Held,
 79 2005), we adopt an idealized dry dynamical core that allows for a bias correction of the
 80 mean flow structure without physical parameterizations. This approach allows us to iso-
 81 late the role of intrinsic planetary waves in the evolution of extreme events.

82 2 Data and Methods

83 2.1 Reanalysis products

84 For the observational analysis, the NCEP/NCAR reanalysis of the National Oceanic
 85 and Atmospheric Administration (NOAA) was implemented. The surface air temper-
 86 ature (SAT), all levels of temperature and the meridional and zonal components of the
 87 wind at 300 hPa (V_{300} and U_{300}) were obtained from these databases with a spatial res-
 88 olution of 2.5° and daily temporal resolution from 1948 to 2023.

89 2.2 An Idealized GCM with realistic climatological basic state

90 Idealized general circulation models are commonly used for the study of atmospheric
 91 dynamics. A dry dynamical core model solves the primitive equations on the sphere by
 92 nudging the climatological temperature field toward a prescribed structure of radiative
 93 equilibrium temperature (T_{eq}). Essentially, this process isolates the dry atmospheric dy-
 94 namics from the complex physical parameterizations.

95 We use the open-access updated version from (Wu & Reichler, 2018) of the spec-
 96 tral dynamical core model proposed by (Held & Suarez, 1994) for the Geophysical Fluid
 97 Dynamics Laboratory (GFDL). The model has a horizontal resolution of T42 (64x128
 98 grid) and 40 vertical σ levels between the surface and 0.01 hPa. To represent the boundary-
 99 layer friction, Rayleigh drag is used to remove momentum in the lower troposphere be-
 100 tween the surface and $\sigma = 0.7$. By default configurations of this model, the tempera-
 101 ture is forced by Newtonian relaxation toward a prescribed equilibrium temperature as
 102 follows:

$$\frac{\partial T}{\partial t} = \frac{T - T_{eq}}{\tau} \quad (1)$$

103 where τ is the prescribed relaxation timescale.

104 Since the primary purpose of this study is to examine how the atmospheric basic
 105 state controls the large-scale Rossby Wave pattern with a zonal wavenumber five struc-

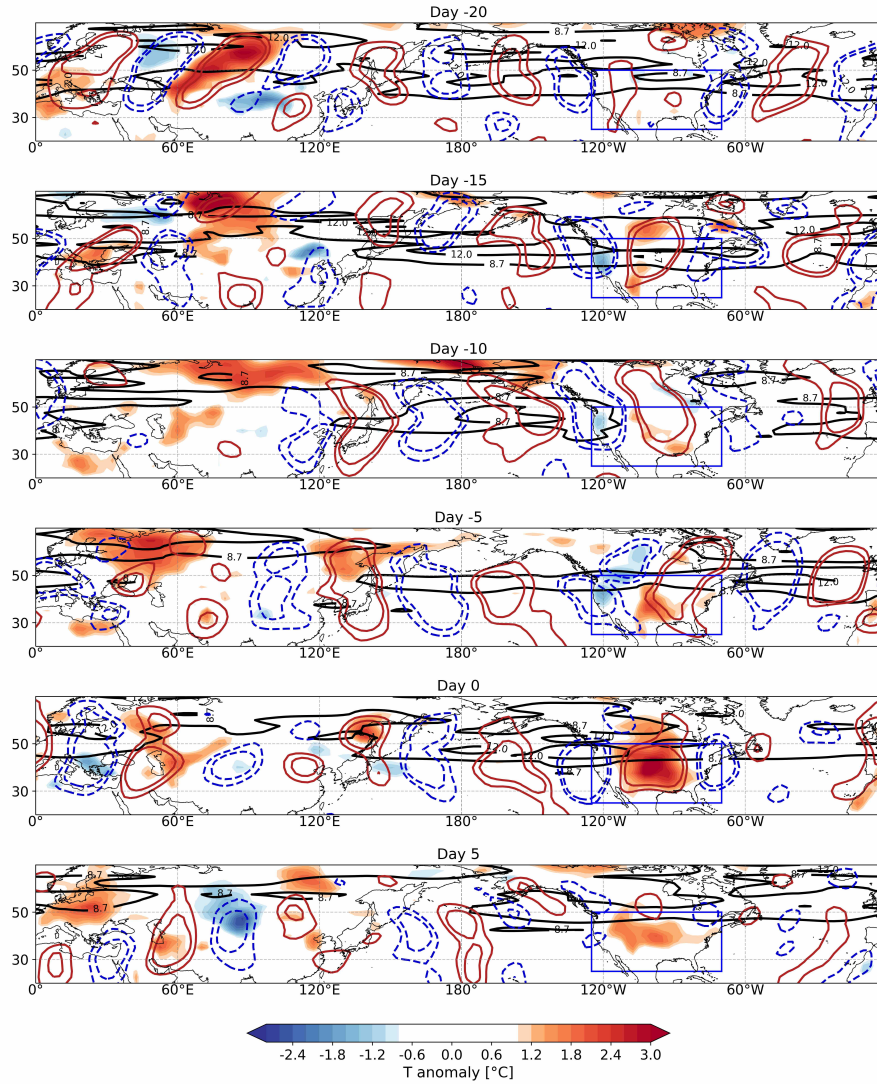


Figure 1. Evolution of heat waves 20 days ahead of the events: Red and dashed blue contours represent composites of 200hPa streamfunction anomalies at ± 0.05 , 0.08 (red as positives). Shading represents surface air temperature anomaly and black contours represent the Rossby Wave Packet envelope at levels 8.7, 12 m/s.

106 ture driving local heat waves in the US, the model includes the iterative procedure pro-
 107 posed by Chang (2006) to simulate the climatological basic state of the atmosphere in
 108 the idealized model. This consists of iterating the radiative equilibrium temperature pro-
 109 file so that at the end of the iterations, the model climate closely resembles the desired
 110 target climate (see Supporting Information for more details of the methodology). The
 111 iteration uses a fixed equilibrium temperature for each N step (T_{eq}) in a run of 62 years,
 112 for a total of 21630 days after eliminating the first 1000 days of simulation. Then, we
 113 calculate the model simulated temperature climatology $T_{(N)}$ and correct it concerning
 114 basic state from the NCEP reanalysis data T_R . The next iteration step N+1 is calcu-
 115 lated according to:

$$T_{eq(N+1)} = T_{eq(N)} - \frac{2}{3}(T_{(N)} - T_R), N = 1, 2, 3... \quad (2)$$

116 To assess the role of the climatological basic state, we carry out three experiments
 117 as follows:

- 118 • **Held and Suarez 1994 configuration (CTR)**: the zonal-mean temperature
 119 structure is relaxed toward a prescribed equinoctial radiative-equilibrium state.
 120 It's the default configuration described in detail in (Held & Suarez, 1994) and leads
 121 to a climatological state close to the observed annual mean climatological state.
- 122 • **Zonally-symmetric boreal summer (ZOB)**: The radiative forcing T_R described
 123 in section 2.2 and in eq. 2 is set by the two-dimensional (i.e., latitude-pressure)
 124 basic state from the NCEP reanalysis data. For this experiment, we use the zon-
 125 ally symmetrical distribution of temperature for the climatological boreal sum-
 126 mer (June, July, and August) between 1948 and 2021.
- 127 • **Realistic Northern Hemisphere summer (ROB)**: The full three-dimensional
 128 structure of the radiative forcing T_R is obtained from the climatological boreal sum-
 129 mer from NCEP, especially including zonal asymmetries. This bias correction in-
 130 cludes zonal variations in T_{eq} , which can be related to zonal variations in diabatic
 131 heating as discussed in Chang (2006) work.

132 2.3 Heat waves identification

133 A heatwave event is set as at least five consecutive days with more than around
 134 900000 km^2 over the US continental area (125W – 70W, 25N – 50N) with daily aver-
 135 aged *SAT* exceeding a threshold value, and the center of these warm points, considered
 136 as the point of maximum temperature, does not move faster than 5 latitude or longitude
 137 per day. The temperature threshold varies spatially as well as with the day of the year.
 138 It was established as the percentile 97.5 of the historical *SAT*. This approach follows
 139 Teng et al. (2013).

140 2.4 Rossby Wave Packets evolution

141 As this study aims to understand the dynamics behind heat waves, it is necessary
 142 to look at the evolution of the Rossby Waves Packets driving extreme events from ob-
 143 servational data and modeling outputs. Both the eddy phase speeds and their group ve-
 144 locity are important physical properties of Rossby Wave Packets' propagation. In par-
 145 ticular, the eddy phase speed indicates the propagation speed of individual troughs within
 146 Rossby Waves Packets. It can thus be critical for the persistence of extreme surface weather
 147 (Röthlisberger et al., 2019). On the other hand, the group velocity reflects how quickly
 148 the whole packet propagates locally and represents the rate at which the Rossby waves
 149 transfer energy horizontally (Pedlosky, 2003). Based on the Rossby Waves Packets' pro-
 150 gression in longitude and time, we compute the envelope of the meridional wind indi-
 151 cating their preferred regions of formation and decay. Specifically, we estimate the Rossby

152 Waves Packets' propagation by constructing Hovmöller diagrams using streamfunction
 153 anomalies at 300 hPa and the corresponding Rossby Waves Packets' envelope.

154 Subsequently, we calculate the local (in space and time) group velocity using the
 155 Rossby Waves Packets' envelope, which reflects how the flow features of enhanced merid-
 156 ional wind amplitude propagate in the zonal and meridional directions (Fragkoulidis &
 157 Wirth, 2020). We implemented the method proposed by Zimin et al. (2003) for the cal-
 158 culation of Rossby Waves Packets' envelope involving the Hilbert transform along cir-
 159 cles of constant latitude combined with a restriction of the zonal wavenumber to a spec-
 160 ified interval, which in this case corresponds to wavenumbers between 3 and 11. We im-
 161 plement this methodology using the meridional wind, which is usually implemented for
 162 the diagnosis of meridional deviations from the zonal flow, and is particularly well suited
 163 for the detection of Rossby waves. Specifically, we take the upper-tropospheric (300 hPa)
 164 meridional wind which features strong Rossby Waves Packet's activities (Wirth et al.,
 165 2018). The meridional wind anomaly $v(x)$ is considered on an equidistant grid along a
 166 latitude circle, where $x = 2\pi/N$ with $0 < x \leq 2\pi$, N is an even integer, and $l = 1, 2, \dots, N$.
 167 The Fourier transform of the real function $v(x)$ is computed as:

$$\hat{v}_k = \frac{1}{N} \sum_{l=1}^N v\left(\frac{2\pi l}{N}\right) e^{-2\pi i k l / N}, \left(K = -\frac{N}{2} + 1, \dots, \frac{N}{2}\right) \quad (3)$$

168 The inverse Fourier transform is applied to a selected band of the positive wavenum-
 169 ber half of the Fourier spectrum:

$$w\left(\frac{2\pi l}{N}\right) = 2 \sum_{k=k_{min}}^{k_{max}} \hat{v}_k e^{2\pi i k l / N} \quad (4)$$

170 Finally, the packet envelope is calculated as follows:

$$A(2\pi l / N) = |w(2\pi l / N)| \quad (5)$$

171 3 Results

172 3.1 Stationary waves preceding heat waves in reanalysis

173 From the reanalysis data, we found 165 heat waves days from 26 events found in
 174 the 75 summers from NCEP. We look at the temporal evolution of the planetary waves
 175 preceding the events by constructing composites from day -20 to day 5 (Figure 1), where
 176 we designate the first day of a heatwave as day 0. We used daily sub-seasonal anom-
 177 alies at 300 hPa streamfunction calculated as the daily departures from the long-term mean
 178 and from the seasonal (June-July-August) mean of the particular year. These anom-
 179 alies were spatially filtered, considering only wavelengths between 2800 km and 10000 km
 180 to consider only the wavenumbers of interest and avoid noise. Defined low and high-pressure
 181 centers can be seen moving slowly westward, expected behavior for Rossby Wave prop-
 182 agation in the days leading up to the extreme event. Although several of the troughs and
 183 ridges are clearly seen, it cannot be readily determined whether the wavenumber is 5 or
 184 6. This difficulty may be explained by the scarcity of the events in the reanalysis, which
 185 are rare by definition. On the other hand, the Rossby Waves amplitudes shown by the
 186 envelope reflect the energy transport by the propagating waves. Notably, the large am-
 187 plitudes of the envelope are seen in the two ocean basins, consistent with the zones where
 188 the Rossby Waves tend to reach large amplitudes and phase speeds. (Fragkoulidis & Wirth,
 189 2020).

190

3.2 Climatology on the idealized simulations

191

192

193

194

195

196

197

198

199

200

201

202

203

204

205

We first discuss the climatological circulation characteristics obtained for the 21630 analyzed days in each experiment (See Supporting Information Figures S1. and S2). As we used a prescribed temperature from NCEP reanalysis data for the Newtonian relaxation in the model, the bias-corrected experiments resemble the zonally symmetric and asymmetric Northern Hemispheric summer in the real atmosphere by construction. It means the temporal mean of the spatial distribution of the temperature, the barotropic averaged zonal wind, and the vertical distribution of the zonal wind, in general, resemble the atmosphere. It should be clarified that although some features of the corrected climatological state are not realistic, especially in the vertical distribution, they are realistic for the key latitudes of interest in this work (between 30°N and 60°N). Note that the basic atmospheric state of the CTR differs spatially and in magnitude from the real atmosphere. While in the real atmosphere, the peak jet intensity is about 10 m/s during the winter, the CTR exhibits a peak of more than 20 m/s. This is because the T_{eq} in the initial configuration is set based on annual climatology values rather than summer seasonality.

206

207

208

209

210

211

212

213

214

215

216

217

218

219

220

221

222

The expected phase speeds corresponding to the climatological zonal winds are calculated for different wavenumbers and compared to the results from reanalysis for the boreal summer (Figure 2). This is to elucidate the expected stationarity for the wave tracks preceding the events. The wavenumbers 5 and 6 have phase speeds close to zero for both observations and the bias-corrected experiments ZOB and ROB. From this calculation, we expect that any pattern associated with any of these wavenumbers can be developed before the events in the corrected experiments. However, the wavenumber five tends to precede U.S. heat waves (Teng et al., 2013). Although in this result for NCEP, it is wave number 6 that has phase velocity closest to 0, it should be noted that although the Rossby wave dispersion relation delves into the large-scale dynamics of mid-latitudes, it is based on a linearized approximation of the equations of motion, and may not accurately represent the behavior of atmospheric waves in situations where nonlinear interactions and other complicating factors are important. On the other hand, the overly strong eddy phase speed obtained for the CTR run again reflect the unrealistic climatology compared to the boreal summer, which provides a non-favorable large-scale environment for developing surface heatwaves. This explains the scarcity of heatwaves in the CTR.

223

3.3 Heat Waves driven by Intrinsic Planetary Wave pattern

224

225

226

227

228

Now that the model resembles the atmospheric basic state for the boreal summer, we can test our hypothesis that the basic state drives the stationary Rossby Waves propagation hence determining heat waves in the mid-latitudes. We must answer, firstly, if it resembles the actual statistics of heat waves, and secondly, if it resembles the atmospheric pattern preceding the events.

229

230

231

232

233

234

235

236

237

238

239

240

We compared the probability of heat waves days and the probability distribution function (PDF) of the events between the experiments and NCEP (Figure 4). We found 111 events and 765 heat waves days in the bias-corrected symmetrical case and 65 and 464 heat waves days in the asymmetric one. Both bias-corrected experiments resemble the PDF of the duration of the events in the reanalysis. However, only the one considering asymmetries (ROB) has a probability of occurrence of heat waves days similar to that found in the reanalysis. In contrast, the overly strong jetstream in the CTR run experiment can explain the extremely rare of similar heatwaves (only 5 events); the phase speeds of troughs are too high to drive persistent weather conditions. Indeed, by changing the detection methodology for this experiment, we can find slightly more events in the CTR. For example, considering a lower velocity of the center of the warm points or a minimum duration of the events shorter than five days, as shown in (Jiménez-Esteve

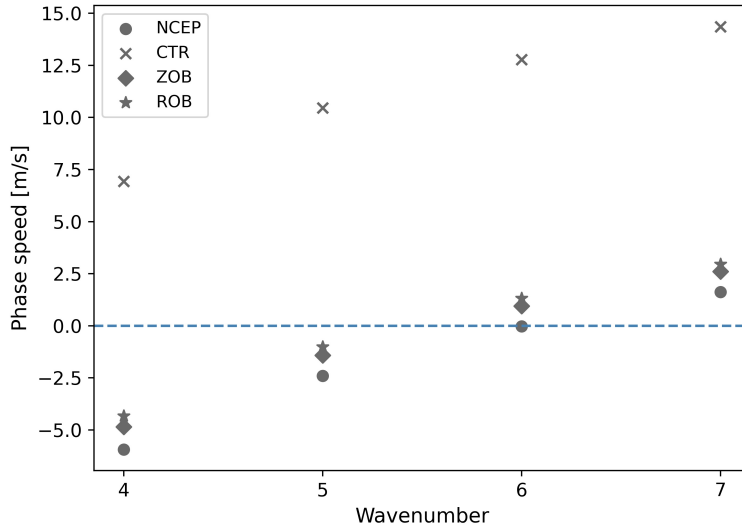


Figure 2. Phase speed for NCEP and the experiments in the Dry Core GCM. Calculated using the Rossby Wave dispersion relation (Eq. 7), considering the maximum barotropic averaged zonal wind in the northern mid-latitudes.

241 & Domeisen, 2022). However, the mere statistical difference of these five events found
 242 with our methodology concerning the event statistics from NCEP and the bias-corrected
 243 ones only confirms that an unrealistic basic state with respect to the boreal summer can-
 244 not provide a conducive environment for developing heatwave events that are statically
 245 consistent with observations.

246 We construct Hovmöller diagrams for streamfunction anomalies and the Rossby
 247 wave envelope for the bias-corrected experiments (Figure 3). In the ZOB and ROB, Rossby
 248 wave propagation along the midlatitudes even 15 days ahead of the events can be ob-
 249 served. It can be seen clearly how the individual troughs and ridges repeatedly amplify
 250 in almost the same longitudinal region, and the envelope shows the slow propagation of
 251 the packets with an overall timescale of 20-30 days. In contrast, all five events in the CTR
 252 are characterized by a much short timescale (3-7 days). Notice that when zonal varia-
 253 tions are included in the experiment ROB, this Hovmöller result has more realistic fea-
 254 tures, and most importantly, the pattern is characterized by a wavenumber 5, which co-
 255 incides with that associated with the occurrence of the events in a realistic atmosphere
 256 (Teng et al., 2013).

257 In addition, the latitudinal location of the jetstream changes for each experiment
 258 and it is known that the jetstream serves as an efficient Rossby waveguide (Hoskins &
 259 Ambrizzi, 1993; Wirth et al., 2018), providing a preferred track for the Rossby Waves.
 260 The waveguide is shifted noticeably upward for the ZOB, while in the ROB, the latitu-
 261 dinal location closely resembles that observed in NCEP. As a consequence, the spatial
 262 location of the events is also more similar to that observed in the reanalysis.

263 *3.3.1 A back-of-the-envelope calculation of the phase speeds*

264 According to the linear wave theory, features of any wave can be derived from its
 265 dispersion relation, which is obtained considering the equation of motion, the assump-
 266 tions of two-dimensional barotropic flow and some other simplifications described in (Vallis,

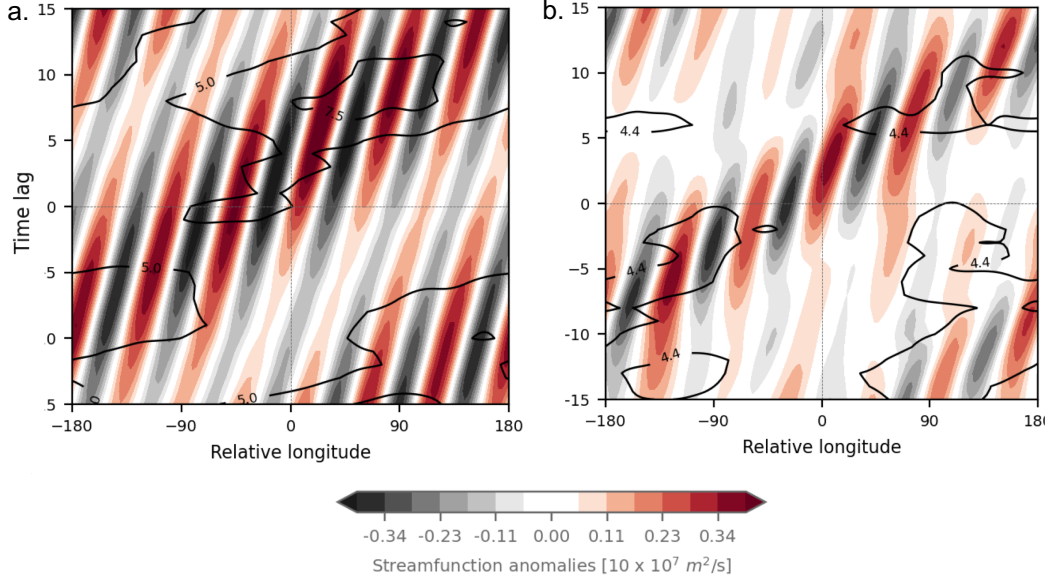


Figure 3. Hövmoller diagrams (longitude - time evolution) for streamfunction anomalies at 300 hPa between 30°N and 50°N with respect to all heatwaves detected (color shading) and Rossby Waves envelope (black contour) for the ZOB experiment (a.) and the ROB experiment (b.).

267 2017). Although these expression come from quite strong approximations, the solutions
 268 turn out to be relevant to the real atmosphere, and provide insight into the large-scale
 269 dynamics of mid-latitudes. The Rossby wave dispersion relation reads as follows:

$$\omega = Uk - \frac{\beta k}{k^2 + l^2} \quad (6)$$

270 Then, the phase speed of Rossby waves in the x direction follows:

$$c_p^x = \frac{\omega}{k} = U - \frac{\beta}{k^2 + l^2} \quad (7)$$

271 Where ω is the constant wave angular frequency in units of radians/time, β the Cori-
 272 olis parameter in β - plane approximation, $k^2 + l^2$ represent the square of the wavevec-
 273 tor, where the wave numbers are given by $k = 2\pi/\lambda_x$, $l = 2\pi/\lambda_y$ with (λ_x, λ_y) the
 274 wavelenghts in units of m. U is the density-weighted zonal-mean zonal-winds at the mid-
 275 latitudes in m/s, for which the density of the air in each layer is calculated considering
 276 the proportionality described in 8, where $z = -H \ln(p/1000hPa)$.

$$\rho \propto e^{-\frac{z}{H}} \quad (8)$$

277 Since the phase speed relative to the background flow is always negative, these waves
 278 always propagate westward relative to the mean flow. When the phase lines are station-
 279 ary relative to the ground, that is, $c_p^x = 0$ (Vallis, 2017), anomalous troughs lead to the
 280 occurrence and persistence of heat waves events.

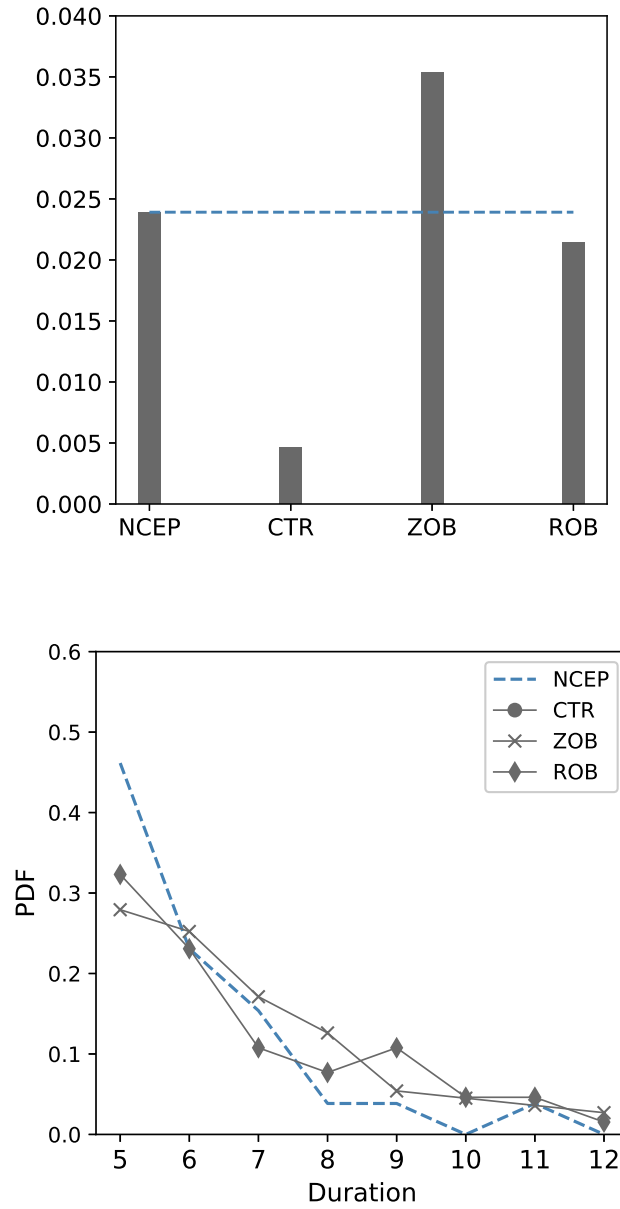


Figure 4. Comparison of statistics between NCEP and the experiments in the dry dynamical core GCM: Number of heatwaves waves over the total of analyzed days (upper) and the probability distribution function (PDF) of the duration of the events (bottom). For the CTR, the only 5 detected events correspond to a duration of 5 days.

4 Conclusions and discussions

The main objective of this study is to understand the role of the basic state on the propagation of Rossby Wave packets driving heat waves in the U.S. We use an idealized atmospheric model where physical parametrizations are substituted by a simple temperature relaxation. We implement the iterative procedure proposed by (Chang, 2006) to simulate the climatological atmosphere for the boreal summer (June, July, August). At the end, the model climate is forced to resemble the observed boreal summer mean flow structure without explicitly considering complicated physical processes (e.g., moisture, turbulence, clouds, etc.). This approach allows us to isolate the dry dynamics aspect of atmospheric circulation on heatwaves evolution, and the conclusions from the results can be summarized as follows:

- The climatological state drives the stationary Rossby wave propagation providing critical dynamical conditions for US heatwaves.
- A dry atmosphere with realistic boreal summer climatological state can produce a wavenumber-five Rossby Waves pattern, which often been seen in the observations preceding US heatwaves.

Previous studies show evidence of heat waves events preceded by a wavenumber five structure contained in Rossby Waves, and the link between the amplification of this pattern with its probability of heatwaves' occurrence. Our study helps to understand the origin of this pattern. It is demonstrated that a dynamical model resembling the actual zonal mean flow (ZOB) can clearly generate a similar Rossby Waves pattern, albeit characterized by zonal wavenumber six, preceding heat waves in the mid-latitudes. However, including the zonal asymmetries in the mean flow (ROB) is crucial for developing the specific wavenumber five structure, and consequently the statistics of the US heatwave events that are consistent with those in reanalysis.

The idealized model enables us to isolate exclusively on the dry atmospheric dynamics to understand the physical mechanism behind the interesting zonal wavenumber five pattern preceding frequent US heatwaves in the summer. While our idealized model contains only dry dynamics, the specific structure of climatological state must arise from the substantial contributions of various diabatic processes. On the one hand, local boundary conditions may play an important role on setting up a realistic climatological state. For example, (Donat et al., 2016; Lyon & Dole, 1995; McKinnon et al., 2016) show that the combination of local anomalous sea surface temperature (*SST*) patterns and atmospheric flow anomalies have contributed significantly to summer extremes. On the other hand, other studies also show the contribution of soil moisture conditions to heat waves by releasing surface diabatic heat (Seneviratne et al., 2010; Miralles et al., 2019) and even to the circumglobal circulation response of Rossby Waves (Douville & Chauvin, 2000; Douville, 2002; Koster et al., 2016). During summer, local land and oceanic conditions are important and may interact nonlinearly with atmospheric circulation states preceding heatwave events. Our next step is to study the dynamics under which local diabatic warming of soil moisture conditions impacts the amplitude of the wave number five pattern and its associated impacts on the statistics of the air temperature extremes in the US.

5 Open Research

The version of the Dry core GCM code used in this work is provided by the open-access data from Wu and Reichler (2018). We constructed the target climatology for our simulations from the NCEP-NCAR Reanalysis 1 data provided by the NOAA PSL, Boulder, Colorado, USA. All the NCEP datasets used for this work can be accessed from <https://downloads.psl.noaa.gov/Datasets/ncep.reanalysis/Dailies/>. The temperature at all levels used to construct the inputs for the simulations, and also the velocity fields used

331 for the comparison are in the folder called *pressure/* in that link, and the temperature
 332 at 2m in the folder *surface_gauss/*. The data also can be downloaded by following the
 333 FTP link in the section Source & References in the NCEP-NCAR Reanalysis 1 webpage:
 334 <https://psl.noaa.gov/data/gridded/data.ncep.reanalysis.html>.

335 The codes for this work and the final datasets obtained from the three simulations
 336 are located in the open-access repository https://github.com/castanev/Dynamics_Heat_Waves.git
 337 linked to Zenodo DOI : 10.5281/zenodo.7844138

338 Acknowledgments

339 The authors acknowledge to NOAA for providing NCEP-NCAR Reanalysis 1 data. They
 340 are also grateful to Zheng Wu and Thomas Reichler for providing openly the code of an
 341 updated version of the GFDL dry dynamical core GCM.

342 References

- 343 Chang, E. K. M. (2006, July). An Idealized Nonlinear Model of the Northern Hemi-
 344 sphere Winter Storm Tracks. *Journal of the Atmospheric Sciences*, *63*(7),
 345 1818–1839. Retrieved 2023-03-24, from [https://journals.ametsoc.org/
 346 view/journals/atsc/63/7/jas3726.1.xml](https://journals.ametsoc.org/view/journals/atsc/63/7/jas3726.1.xml) (Publisher: American Me-
 347 teorological Society Section: Journal of the Atmospheric Sciences) doi:
 348 10.1175/JAS3726.1
- 349 Chen, P., & Newman, M. (1998, October). Rossby Wave Propagation and
 350 the Rapid Development of Upper-Level Anomalous Anticyclones during
 351 the 1988 U.S. Drought. *Journal of Climate*, *11*(10), 2491–2504. Re-
 352 trieved 2023-04-07, from [https://journals.ametsoc.org/view/journals/
 353 clim/11/10/1520-0442_1998_011_2491_rwpatr_2.0.co_2.xml](https://journals.ametsoc.org/view/journals/clim/11/10/1520-0442_1998_011_2491_rwpatr_2.0.co_2.xml) (Pub-
 354 lisher: American Meteorological Society Section: Journal of Climate) doi:
 355 10.1175/1520-0442(1998)011<2491:RWPATR>2.0.CO;2
- 356 Ding, Q., & Wang, B. (2005, September). Circumglobal Teleconnection in the
 357 Northern Hemisphere Summer. *Journal of Climate*, *18*(17), 3483–3505. Re-
 358 trieved 2023-04-07, from [https://journals.ametsoc.org/view/journals/
 359 clim/18/17/jcli3473.1.xml](https://journals.ametsoc.org/view/journals/clim/18/17/jcli3473.1.xml) (Publisher: American Meteorological Society
 360 Section: Journal of Climate) doi: 10.1175/JCLI3473.1
- 361 Donat, M. G., King, A. D., Overpeck, J. T., Alexander, L. V., Durre, I., & Karoly,
 362 D. J. (2016, January). Extraordinary heat during the 1930s US Dust Bowl
 363 and associated large-scale conditions. *Climate Dynamics*, *46*(1), 413–426.
 364 Retrieved 2023-04-07, from <https://doi.org/10.1007/s00382-015-2590-5>
 365 doi: 10.1007/s00382-015-2590-5
- 366 Douville, H. (2002, April). Influence of Soil Moisture on the Asian and African
 367 Monsoons. Part II: Interannual Variability. *Journal of Climate*, *15*(7), 701–
 368 720. Retrieved 2023-04-07, from [https://journals.ametsoc.org/view/
 369 journals/clim/15/7/1520-0442_2002_015_0701_iosmot_2.0.co_2.xml](https://journals.ametsoc.org/view/journals/clim/15/7/1520-0442_2002_015_0701_iosmot_2.0.co_2.xml)
 370 (Publisher: American Meteorological Society Section: Journal of Climate)
 371 doi: 10.1175/1520-0442(2002)015<0701:IOSMOT>2.0.CO;2
- 372 Douville, H., & Chauvin, F. (2000, October). Relevance of soil moisture for seasonal
 373 climate predictions: a preliminary study. *Climate Dynamics*, *16*(10), 719–736.
 374 Retrieved 2023-04-07, from <https://doi.org/10.1007/s003820000080> doi:
 375 10.1007/s003820000080
- 376 Feldstein, S. B. (2000, December). The Timescale, Power Spectra, and Climate
 377 Noise Properties of Teleconnection Patterns. *Journal of Climate*, *13*(24),
 378 4430–4440. Retrieved 2023-03-31, from [https://journals.ametsoc.org/
 379 view/journals/clim/13/24/1520-0442_2000_013_4430_ttpsac_2.0.co_2.xml](https://journals.ametsoc.org/view/journals/clim/13/24/1520-0442_2000_013_4430_ttpsac_2.0.co_2.xml)
 380 (Publisher: American Meteorological Society Section: Journal of Climate) doi:
 381 10.1175/1520-0442(2000)013<4430:TTPSAC>2.0.CO;2

- 382 Fragkoulidis, G., & Wirth, V. (2020, October). Local Rossby Wave Packet Ampli-
 383 tude, Phase Speed, and Group Velocity: Seasonal Variability and Their Role
 384 in Temperature Extremes. *Journal of Climate*, *33*(20), 8767–8787. Retrieved
 385 2023-04-07, from [https://journals.ametsoc.org/view/journals/clim/33/](https://journals.ametsoc.org/view/journals/clim/33/20/jcliD190377.xml)
 386 [20/jcliD190377.xml](https://journals.ametsoc.org/view/journals/clim/33/20/jcliD190377.xml) (Publisher: American Meteorological Society Section:
 387 Journal of Climate) doi: 10.1175/JCLI-D-19-0377.1
- 388 Held, I. M. (2005, November). The Gap between Simulation and Understanding in
 389 Climate Modeling. *Bulletin of the American Meteorological Society*, *86*(11),
 390 1609–1614. Retrieved 2023-04-15, from [https://journals.ametsoc.org/](https://journals.ametsoc.org/view/journals/bams/86/11/bams-86-11-1609.xml)
 391 [view/journals/bams/86/11/bams-86-11-1609.xml](https://journals.ametsoc.org/view/journals/bams/86/11/bams-86-11-1609.xml) (Publisher: Ameri-
 392 can Meteorological Society Section: Bulletin of the American Meteorological
 393 Society) doi: 10.1175/BAMS-86-11-1609
- 394 Held, I. M., & Suarez, M. J. (1994, October). A Proposal for the Intercomparison
 395 of the Dynamical Cores of Atmospheric General Circulation Models. *Bulletin*
 396 *of the American Meteorological Society*, *75*(10), 1825–1830. Retrieved 2023-
 397 03-24, from [https://journals.ametsoc.org/view/journals/bams/75/10/](https://journals.ametsoc.org/view/journals/bams/75/10/1520-0477_1994_075_1825_apftio_2_0_co_2.xml)
 398 [1520-0477_1994_075_1825_apftio_2_0_co_2.xml](https://journals.ametsoc.org/view/journals/bams/75/10/1520-0477_1994_075_1825_apftio_2_0_co_2.xml) (Publisher: American Me-
 399 teorological Society Section: Bulletin of the American Meteorological Society)
 400 doi: 10.1175/1520-0477(1994)075(1825:APFTIO)2.0.CO;2
- 401 Hoskins, B. J., & Ambrizzi, T. (1993, June). Rossby Wave Propagation on a Realis-
 402 tic Longitudinally Varying Flow. *Journal of the Atmospheric Sciences*, *50*(12),
 403 1661–1671. Retrieved 2023-04-07, from [https://journals.ametsoc.org/](https://journals.ametsoc.org/view/journals/atsc/50/12/1520-0469_1993_050_1661_rwpoar_2_0_co_2.xml)
 404 [view/journals/atsc/50/12/1520-0469_1993_050_1661_rwpoar_2_0_co_2.xml](https://journals.ametsoc.org/view/journals/atsc/50/12/1520-0469_1993_050_1661_rwpoar_2_0_co_2.xml)
 405 (Publisher: American Meteorological Society Section: Journal of the Atmo-
 406 spheric Sciences) doi: 10.1175/1520-0469(1993)050(1661:RWPOAR)2.0.CO;2
- 407 Jiménez-Esteve, B., & Domeisen, D. I. (2022, July). The role of atmospheric dynam-
 408 ics and large-scale topography in driving heatwaves. *Quarterly Journal of the*
 409 *Royal Meteorological Society*, *148*(746), 2344–2367. Retrieved 2023-04-07, from
 410 <https://onlinelibrary.wiley.com/doi/10.1002/qj.4306> doi: 10.1002/qj
 411 .4306
- 412 Koster, R. D., Chang, Y., Wang, H., & Schubert, S. D. (2016, October). Impacts of
 413 Local Soil Moisture Anomalies on the Atmospheric Circulation and on Remote
 414 Surface Meteorological Fields during Boreal Summer: A Comprehensive Anal-
 415 ysis over North America. *Journal of Climate*, *29*(20), 7345–7364. Retrieved
 416 2023-04-07, from [https://journals.ametsoc.org/view/journals/clim/](https://journals.ametsoc.org/view/journals/clim/29/20/jcli-d-16-0192.1.xml)
 417 [29/20/jcli-d-16-0192.1.xml](https://journals.ametsoc.org/view/journals/clim/29/20/jcli-d-16-0192.1.xml) (Publisher: American Meteorological Society
 418 Section: Journal of Climate) doi: 10.1175/JCLI-D-16-0192.1
- 419 Lyon, B., & Dole, R. M. (1995, June). A Diagnostic Comparison of the 1980 and
 420 1988 U.S. Summer Heat Wave-Droughts. *Journal of Climate*, *8*(6), 1658–
 421 1675. Retrieved 2023-04-07, from [https://journals.ametsoc.org/view/](https://journals.ametsoc.org/view/journals/clim/8/6/1520-0442_1995_008_1658_adcota_2_0_co_2.xml)
 422 [journals/clim/8/6/1520-0442_1995_008_1658_adcota_2_0_co_2.xml](https://journals.ametsoc.org/view/journals/clim/8/6/1520-0442_1995_008_1658_adcota_2_0_co_2.xml) (Pub-
 423 lisher: American Meteorological Society Section: Journal of Climate) doi:
 424 10.1175/1520-0442(1995)008<1658:ADCOTA>2.0.CO;2
- 425 McKinnon, K. A., Rhines, A., Tingley, M. P., & Huybers, P. (2016, May). Long-
 426 lead predictions of eastern United States hot days from Pacific sea surface
 427 temperatures. *Nature Geoscience*, *9*(5), 389–394. Retrieved 2023-04-07, from
 428 <https://www.nature.com/articles/ngeo2687> (Number: 5 Publisher: Na-
 429 ture Publishing Group) doi: 10.1038/ngeo2687
- 430 Meehl, G. A., & Tebaldi, C. (2004, August). More Intense, More Frequent, and
 431 Longer Lasting Heat Waves in the 21st Century. *Science*, *305*(5686), 994–
 432 997. Retrieved 2023-04-07, from [https://www.science.org/doi/10.1126/](https://www.science.org/doi/10.1126/science.1098704)
 433 [science.1098704](https://www.science.org/doi/10.1126/science.1098704) (Publisher: American Association for the Advancement of
 434 Science) doi: 10.1126/science.1098704
- 435 Miralles, D. G., Gentile, P., Seneviratne, S. I., & Teuling, A. J. (2019, January).
 436 Land–atmospheric feedbacks during droughts and heatwaves: state of the sci-

- 437 ence and current challenges. *Annals of the New York Academy of Sciences*,
438 1436(1), 19–35. Retrieved 2023-04-07, from [https://www.ncbi.nlm.nih.gov/](https://www.ncbi.nlm.nih.gov/pmc/articles/PMC6378599/)
439 [pmc/articles/PMC6378599/](https://www.ncbi.nlm.nih.gov/pmc/articles/PMC6378599/) doi: 10.1111/nyas.13912
- 440 Pedlosky, J. (2003). *Waves in the Ocean and Atmosphere: Introduction to Wave Dy-*
441 *namics* (2003rd edition ed.). Berlin ; New York: Springer.
- 442 Röthlisberger, M., Frossard, L., Bosart, L. F., Keyser, D., & Martius, O. (2019,
443 June). Recurrent Synoptic-Scale Rossby Wave Patterns and Their Effect on
444 the Persistence of Cold and Hot Spells. *Journal of Climate*, 32(11), 3207–3226.
445 Retrieved 2023-04-07, from [https://journals.ametsoc.org/view/journals/](https://journals.ametsoc.org/view/journals/clim/32/11/jcli-d-18-0664.1.xml)
446 [clim/32/11/jcli-d-18-0664.1.xml](https://journals.ametsoc.org/view/journals/clim/32/11/jcli-d-18-0664.1.xml) doi: 10.1175/JCLI-D-18-0664.1
- 447 Schubert, S., Wang, H., & Suarez, M. (2011, September). Warm Season Subseasonal
448 Variability and Climate Extremes in the Northern Hemisphere: The Role of
449 Stationary Rossby Waves. *Journal of Climate*, 24(18), 4773–4792. Retrieved
450 2023-04-15, from [https://journals.ametsoc.org/view/journals/clim/24/](https://journals.ametsoc.org/view/journals/clim/24/18/jcli-d-10-05035.1.xml)
451 [18/jcli-d-10-05035.1.xml](https://journals.ametsoc.org/view/journals/clim/24/18/jcli-d-10-05035.1.xml) (Publisher: American Meteorological Society
452 Section: Journal of Climate) doi: 10.1175/JCLI-D-10-05035.1
- 453 Seneviratne, S. I., Corti, T., Davin, E. L., Hirschi, M., Jaeger, E. B., Lehner, I., . . .
454 Teuling, A. J. (2010, May). Investigating soil moisture–climate interactions
455 in a changing climate: A review. *Earth-Science Reviews*, 99(3), 125–161.
456 Retrieved 2023-04-15, from [https://www.sciencedirect.com/science/](https://www.sciencedirect.com/science/article/pii/S0012825210000139)
457 [article/pii/S0012825210000139](https://www.sciencedirect.com/science/article/pii/S0012825210000139) doi: 10.1016/j.earscirev.2010.02.004
- 458 Teng, H., Branstator, G., Wang, H., Meehl, G. A., & Washington, W. M. (2013,
459 December). Probability of US heat waves affected by a subseasonal planetary
460 wave pattern. *Nature Geoscience*, 6(12), 1056–1061. Retrieved 2023-03-24,
461 from <https://www.nature.com/articles/ngeo1988> (Number: 12 Publisher:
462 Nature Publishing Group) doi: 10.1038/ngeo1988
- 463 Vallis, G. K. (2017). *Atmospheric and Oceanic Fluid Dynamics: Funda-*
464 *mentals and Large-Scale Circulation* (2nd ed.). Cambridge: Cambridge
465 University Press. Retrieved 2023-03-01, from [https://www.cambridge](https://www.cambridge.org/core/books/atmospheric-and-oceanic-fluid-dynamics/41379BDDC4257CBE11143C466F6428A4)
466 [.org/core/books/atmospheric-and-oceanic-fluid-dynamics/](https://www.cambridge.org/core/books/atmospheric-and-oceanic-fluid-dynamics/41379BDDC4257CBE11143C466F6428A4)
467 [41379BDDC4257CBE11143C466F6428A4](https://www.cambridge.org/core/books/atmospheric-and-oceanic-fluid-dynamics/41379BDDC4257CBE11143C466F6428A4) doi: 10.1017/9781107588417
- 468 Wirth, V., Riemer, M., Chang, E. K. M., & Martius, O. (2018, July). Rossby Wave
469 Packets on the Midlatitude Waveguide—A Review. *Monthly Weather Review*,
470 146(7), 1965–2001. Retrieved 2023-04-05, from [https://journals.ametsoc](https://journals.ametsoc.org/view/journals/mwre/146/7/mwr-d-16-0483.1.xml)
471 [.org/view/journals/mwre/146/7/mwr-d-16-0483.1.xml](https://journals.ametsoc.org/view/journals/mwre/146/7/mwr-d-16-0483.1.xml) (Publisher: Amer-
472 ican Meteorological Society Section: Monthly Weather Review) doi: 10.1175/
473 MWR-D-16-0483.1
- 474 Wu, Z., & Reichler, T. (2018). Towards a more earth-like circulation in idealized
475 models. Retrieved from <https://doi.org/> doi: 10.1029/2018MS001356
- 476 Zimin, A. V., Szunyogh, I., Patil, D. J., Hunt, B. R., & Ott, E. (2003, May). Ex-
477 tracting Envelopes of Rossby Wave Packets. *Monthly Weather Review*, 131(5),
478 1011–1017. Retrieved 2023-03-24, from [https://journals.ametsoc.org/](https://journals.ametsoc.org/view/journals/mwre/131/5/1520-0493_2003_131_1011_eeorwp_2.0.co_2.xml)
479 [view/journals/mwre/131/5/1520-0493_2003_131_1011_eeorwp_2.0.co_2.xml](https://journals.ametsoc.org/view/journals/mwre/131/5/1520-0493_2003_131_1011_eeorwp_2.0.co_2.xml)
480 (Publisher: American Meteorological Society Section: Monthly Weather Re-
481 view) doi: 10.1175/1520-0493(2003)131<1011:EEORWP>2.0.CO;2